Design optimization of a latent heat storage using sodium acetate trihydrate

Wang, Gang; Liao, Zhirong; Xu, Chao; Englmair, Gerald; Kong, Weiqiang; Fan, Jianhua; Wei, Gaosheng; Furbo, Simon

Published in:
Journal of Energy Storage

Link to article, DOI:
10.1016/j.est.2022.104798

Publication date:
2022

Document Version
Publisher's PDF, also known as Version of record

Journal of Energy Storage 52 (2022) 104798

Contents lists available at ScienceDirect

Journal of Energy Storage

journal homepage: www.elsevier.com/locate/est

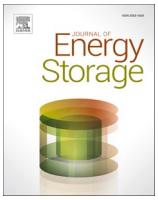

Research papers

Design optimization of a latent heat storage using sodium acetate trihydrate

Gang Wang [a,b], Zhirong Liao [a], Chao Xu [a], Gerald Englmair [b], Weiqiang Kong [b], Jianhua Fan [b,*], Gaosheng Wei [a], Simon Furbo [b]

[a] Key Laboratory of Condition Monitoring and Control for Power Plant Equipment of MOE, North China Electric Power University, Beijing 102206, PR China
[b] Department of Civil Engineering, Technical University of Denmark, Brovej 11, 2800 Kgs. Lyngby, Denmark

ARTICLE INFO

Keywords:
Phase change material
Flexible heat storage
CFD simulation
Thermal characteristic
Design optimization

ABSTRACT

This paper presents numerical investigations on a heat storage utilizing sodium acetate trihydrate (SAT) as phase change material (PCM). The heat storage can be used both in short-term and in long-term by utilizing stable supercooling of SAT. The store contains 137.8 kg PCM and 75 L water. Based on a validated CFD model, the flow conditions of the heat storage was analyzed. Uneven flow distribution inside the heat storage was revealed. Three design optimization methods were investigated to eliminate the uneven flow distribution. The results were analyzed using key performance indicators inclusive charging time, charged heat, degree of thermal stratification and the mixing of the heat storage. The influence of flow direction, inlet size and addition of a porous plate on the thermal performance of the heat storage were elucidated. Concerning flow direction, after moving the inlet from the bottom to the top of the storage, the time needed to completely melt the PCM was shortened by 50%. The best storage design was identified: For charge of the storage, the top inlet should be used, while for discharge, the bottom inlet should be used. Concerning the size of inlet opening, the charging time of the heat storage was reduced from 75 min to 51 min by using 3.0 mm radius instead of a 11.2 mm inlet. The small inlet size (3.0–8.0 mm) was suggested to make a uniform temperature distribution inside the heat storage. Short circuit was completely eliminated by adding a porous plate with 10% porosity. The charging time of the heat storage was shortened 28% by adding the porous plate. Finally, recommendations were proposed for different applications of the heat storage. The findings of the paper serve as a good basis for designers and manufacturers of PCM heat storages.

1. Introduction

Carbon dioxide is considered as one of the main reasons for the climate change and extreme weather [1]. In 2018, totally 33.9 Gt of CO_2 were emitted globally [2]. Carbon emissions from burning of fossil fuels are the largest source of greenhouse gas emissions.

Limiting carbon dioxide emission is the key method to achieve the 2 °C climate target [3]. Carbon neutrality target is one of the most popular topics in the world. More and more countries have announced their plans to peak carbon dioxide emission and carbon neutrality. Until 2010, 49 countries have already passed peak levels of green gas emission [4], including Germany, Russia, Finland, Denmark, etc. In September of 2020, Chinese government declared that China would scale up its nationally determined contributions and adopt more vigorous policies and measures to peak carbon dioxide emissions before 2030 and achieve carbon neutrality before 2060 at the General Debate of the 75th Session of the United Nations General Assembly [5].

Increasing the use of renewable energy including solar, wind, biomass, hydro, tidal, wave, and geothermal energy is recognized as an effective way to achieve the carbon neutrality [6]. Due to the advantages such as inexhaustible, non-polluting, and clean, solar energy is one of the most important renewable energies which will be developed vigorously [7]. Increasing the usage of solar energy is a key method for reducing carbon dioxide emission [8]. However, naturally uncertainty, instability, and intermittently of solar irradiation are limitations for the application of solar energy utilization [9].

Adding a thermal energy storage is an effective way to provide a stable solar heat supply [10]. Thermal energy storage (TES) is the main energy storage technology due to its low cost, security and flexibility. With TES systems, the efficiency and reliability of the solar heating systems will be improved significantly [11].

* Corresponding author.
E-mail address: jif@byg.dtu.dk (J. Fan).

https://doi.org/10.1016/j.est.2022.104798
Received 24 February 2022; Received in revised form 24 April 2022; Accepted 2 May 2022
Available online 11 May 2022

1.1. PCM heat storage

Due to its high latent heat [12] and constant charging/discharging temperature [13], phase change materials (PCM) are recognized as promising thermal energy storage materials. PCMs are widely used not only in solar energy system and industrial waste heat recovery systems, but also in food packaging, clothing and green building fields [14].

Applications of PCM in TES systems are mainly focused on short-term heat storages. However, due to the high cost of PCM, the application of PCM is still not popular [15]. Using PCM as a long-term heat storage is possible due to the supercooling characteristic of some special PCMs [16]. A large amount of heat can be stored as latent heat in the supercooled liquid phase PCM. By controlled solidification of the liquid PCM, the stored heat can be released and utilized on demand, thus achieving a flexible long-term heat storage. Sodium acetate trihydrate (SAT) is a salt hydrate with many advantages such as high latent heat, small phase change expansion coefficient, excellent chemical stability, non-toxicity, low-cost and being easily accessible. The melting point of SAT (58 °C) is suitable for space heating system and domestic hot water supply. The supercooling of SAT is able to be stabilized by adding additives. Long-term heat storage utilizing stable supercooling of SAT has been experimentally investigated and verified [17].

Stable supercooling was achieved for composites of SAT and thickening agents. In the experiment of Zhou et al. [18,19], stable supercooling (more than 35 h) of SAT-water mixtures was successfully achieved. In the experiment of Yuan et al. [20], after adding acetic acid into SAT, a long-term supercooling (more than 14 days) was achieved at room temperature. Similarly, in the experiments of Johansen et al. [21], the supercooling of SAT-2.0 wt% CMC-5.0 wt% graphite powder composite was very stable (more than 5 months).

The long-term thermal performances of two flat chambers with SAT-based PCM were investigated by Dannemand et al. [22]. The total heat capacity of these two flat chambers were 147 kWh/m^3 and 173 kWh/m^3, the long-term heat capacity were 57 kWh/m^3 and 73 kWh/m^3 (15–90 °C). Englmair et al. [23] investigated the thermal performance of long-term flat chamber heat storage. The flat chambers were filled with different PCMs. The total heat capacity of the three flat chambers were all around 160 kWh/m^3, and the long-term heat capacity of these three flat chambers was 51 kWh/m^3, 54 kWh/m^3 and 60 kWh/m^3 respectively. A segmented long-term heat storage with four flat chambers was investigated under Danish weather conditions [24], and its maximum charging and discharging power was 36 kW and 6 kW. Based on the experiment, in spring and autumn, the SAT heat storage was efficiently retrieved to provide thermal energy to the heating system.

1.2. Design optimization

Adding fins in a heat storage is a simple and effective way to enhance the heat transfer of the heat storage. The effects of different types of fins have been widely investigated. The effect of annular fins on a shell-and-tube storage unit was simulated, modeled and optimized by Elmaazouzi et al. [25]. After integrating the annular fins, the charging time of the heat storage was shortened by 65% and the discharging time was shortened by 58%. Kirincic et al. [26] investigated the effect of longitudinal fins on the thermal performance of a latent heat storage. After installing longitudinal fins, the total melting time and solidification time of the heat storage was reduced by 52% and 43% respectively.

Wu et al. [27] designed a unequal-length compensating fin, after adding the fins into a latent heat storage, the melting and solidification time of the heat storage was shortened by 64% and 82%, respectively. The unequal-length compensating fin increased the heat transfer rate by 155%. Yu et al. [28] proposed that compared with the plate fins, adding tree-like fins in latent heat storage achieved better melting rate and temperature distribution under high heat flow condition. The melting time of the latent heat storage was shortened 27% by the tree-like fins.

The design of the heat storage has obvious influence on its thermal performance. Lamrani et al. [29] investigated the effect of tube number on the thermal performance of a shell and tube heat storage. The produced thermal energy from the PCM storage was increased from 90 kWh to 178 kWh in 7 h with the increase of the number of tubes from 200 tubes to 500 tubes in the storage unit while maintaining the same amount of PCM. Joshi et al. [30] added porous flow distributor into a single media heat storage tank to improve its thermal stratification. The results showed that the permeability of the flow distributor in the range between 10^{-9} m^2 and 10^{-8} m^2, leaded to the best thermal stratification. Weiss et al. [31] also added a fluid distributor inside a heat storage and analyzed the influence of the fluid distributor location on the thermal stratification of the heat storage. The results of the analysis showed that the fluid distributor should always be located in the upper-most part of the tank to minimize the initial thermocline thickness.

1.3. Aim and scope

A heat storage combining short-term and long-term heat storage was investigated by the authors for green buildings and renewable energy systems [32]. The heat storage was designed and constructed by H.M. Heizkörper, and 137.8 kg PCM and 75 L water were filled in the heat storage (Figs. 1 and 2). The design of the heat storage is chosen for single family applications. Detailed information on the heat storage design can be found in the published work of the authors [17]. It was shown that the

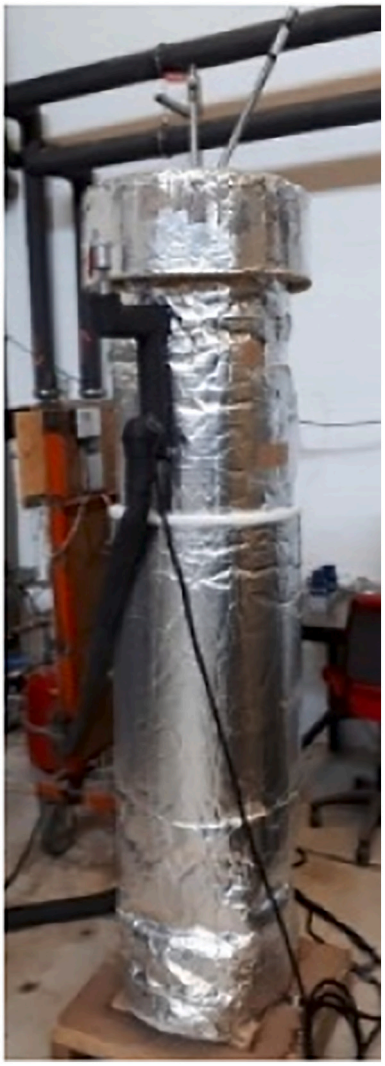

Fig. 1. The investigated heat storage [17].

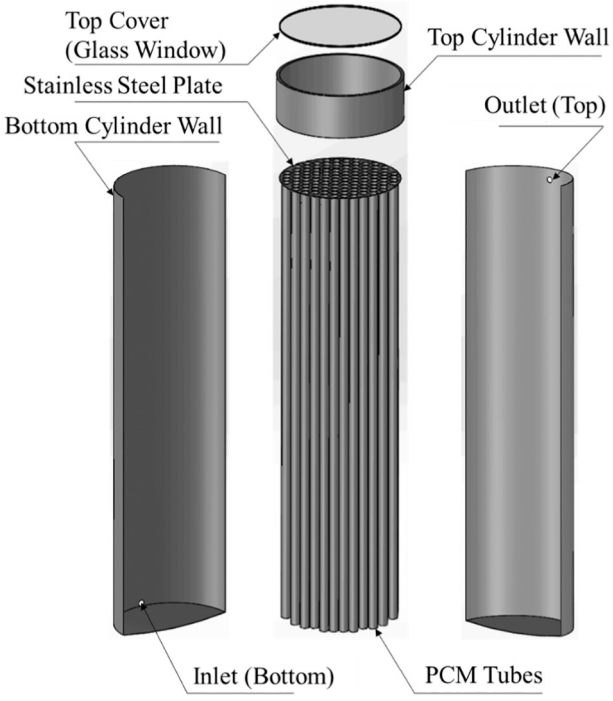

Fig. 2. A break-down drawing of the heat storage [32].

design of the heat storage is not optimal, due to unwanted mixing/flow short circuit in the tank. In the charging process, a fluid short circuit existed inside the water region. Part of hot water flows out of the heat storage before sufficiently releasing its heat [32]. To achieve a better thermal performance, the hot water short circuit and the uneven flow distribution in the tank should be eliminated.

The aim of this paper is to try to tackle the critical problem of uneven flow distribution in the heat storage with minimum cost. Design of the heat storage will be optimized by minimizing the unwanted mixing/flow short circuit in the tank. The flow conditions of the heat storage was analyzed by CFD calculations. The added values of the paper are:

1. The uneven flow distribution inside the heat storage was revealed. Three improved storage designs were suggested and investigated to eliminate the short circuit flow and to improve the thermal performance of the heat storage.
2. Four key thermal performance indicators inclusive charging time, charged heat, degree of thermal stratification and the mixing of the heat storage are used to examine the storage designs. The mixing of the heat storage is defined as the stirring of the PCM inside the heat storage by natural convection. A major advantage of the investigated heat storage is the self-stirring function for liquid PCM, since the arrangement of the inlet at the bottom and the outlet at the top of the heat storage creates a "top-low and bottom-high" temperature distribution in the heat storage during charging. Consequently, the bottom of the tube is heated with a higher temperature than the top of the tube. Temperature driven convection flow of the liquid PCM is formed in the tube, resulting in a good degree of mixing of PCM in the tube. Water molecules combine with sodium acetate to form SAT, preventing phase separation of SAT and improving long term stability of the heat storage. The stirring of PCM during charging is used as one of the key criteria in evaluation of the storage designs.
3. The influence of flow direction, inlet size and porous plate on the thermal performance of the heat storage are elucidated.
4. Finally, recommendations are given for different application scenarios of the heat storage.

This research is part of the Danish Energy Agency EUDP project on participation of the IEA Task 58 'Material and Component Development for Thermal Energy Storage'. The findings of the project serve a good reference for researchers, designers and manufacturers of PCM heat storages.

2. The uneven flow distribution and design improvements

2.1. Short circuit flow inside the storage

The flow characteristics of water and liquid PCM were revealed by the CFD calculations in the previous publication [32]. In the charging process, the fluid short circuit existed in the water region, shown as Fig. 3. Part of the incoming hot water flow out of the tank without releasing heat sufficiently. There was no obvious thermocline inside the tank during charge. Some tubes were heated directly by hot water, while other tubes were heated by the reverse flow. The hot water short circuit flow during charge is a problem which needs to be eliminated.

2.2. Improved designs

The above mentioned short circuit flow is mainly related to the design of the heat storage. To eliminate the short circuit flow, the design of the heat storage needs to be improved. The following design improvement methods were suggested and analyzed (Fig. 4):

In Method A, the flow direction is changed so that high temperature water enters through the top inlet. Two different working modes were analyzed and compared. The heat storage with the top inlet is named Top Inlet Mode, while the heat storage with the bottom inlet is named Bottom Inlet Mode. When using different modes, the flow direction will be changed in the whole working cycle "charge-discharge of sensible heat-discharge of latent heat". The influence of flow direction was analyzed in the charging process, the discharging of sensible heat process and the discharging of latent heat process. The details of the simulations are shown in Table 1.

In the Method B, the size of the bottom inlet is changed. Small inlet sizes were used to form jet flow to increase the temperature uniformity of the heat storage. Totally 6 different inlet sizes were analyzed and divided into two groups. The details of the different inlet sizes are shown in Table 2. In the investigations, the original heat storage design is used meaning that the inlet was at bottom and only the inlet size was changed. Due to the fact that the flow direction was not changed, the short-circuit flow only appeared in the charging process. The influence of inlet size was only analyzed for the charging process.

In Method C, a porous plate was added in the heat storage below the PCM tubes. It is expected that the porous plate will equalize flow in the horizontal section plane of the heat storage. The parameters of the added porous plate are shown in Table 3. Similar to Method B, the analysis of this method was only investigated for the charging process.

In all the simulations, the heating temperature was 92 °C (365 K) and

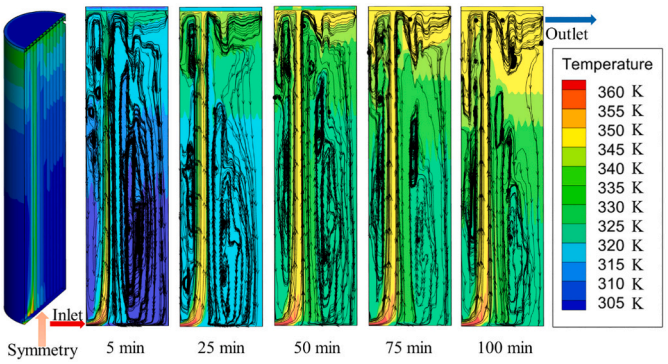

Fig. 3. The water flow pattern inside the heat storage during charge [32].

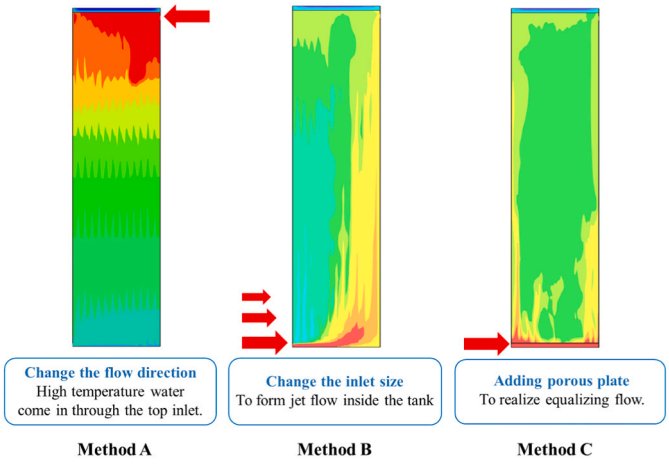

Fig. 4. Schematics of three design optimizations.

Table 1
Details of different HTF flow direction modes.

Cases	Process	Modes	Inlet Temperature
Case A-1	Charge	Top Inlet	92 °C
Case A-2	Charge	Bottom Inlet[a]	92 °C
Case A-3	Discharge of sensible heat	Top Inlet	30 °C
Case A-4	Discharge of sensible heat	Bottom Inlet[a]	30 °C
Case A-5	Discharge of latent heat	Top Inlet	30 °C
Case A-6	Discharge of latent heat	Bottom Inlet[a]	30 °C

[a] Original case.

Table 2
The parameter of different inlet sizes.

Group	Cases	Radius of inlet (mm)
Small inlet group	Case B-7	3.0
	Case B-8	5.0
	Case B-9	8.0
Large inlet group	Case B-10	10.0
	Case B-11[a]	11.2
	Case B-12	12.0

[a] Original case.

Table 3
The parameter of the porous plate.

Cases	Thickness (mm)	Porosity (–)	Pore Size (mm)	Viscous Resistance (m^{-2})	Inertial Resistance (m^{-1})
Case C-13	Non Porous Plate – Original Case				
Case C-14	2	0.1	2	3.038×10^{10}	1.575×10^{6}

the hot water flow rate was 14 L/min. The aims of the improvements are eliminating the short circuit, increasing the uniformity of the temperature distribution, increasing the charging rate and realizing the stirring.

3. CFD model and methodology

The structured mesh was adopted in this model (totally 1.38×10^7 cells), the mesh skewness of the model was 0.64. To ensure the accuracy of the simulations, the boundary layers were added in the model both inside and outside of the tubes. The CFD model was imported into Fluent to carry out the numerical simulations. The generated mesh is shown in Fig. 5.

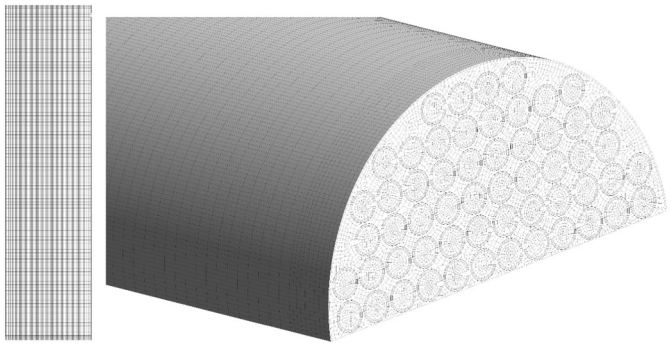

Fig. 5. The generated mesh used in CFD simulation (left: vertical middle cut plane, right: horizontal cut plane).

3.1. The governing equations

The governing equations of the solidification and melting model have been introduced in the previous publication [32] in detail. For the simulation process solver equation, the following assumptions are considered:

- The working fluid (both PCM and water, the heat transfer fluid) is incompressible.
- The crystallization occurred simultaneously in the whole volume.
- The thermophysical properties of PCM are independent of temperature.
- The volume of PCM does not change in the phase change process.

The following simulation settings were used. The Boussinesq approximation was used to calculate the buoyancy-driven forces [33]. The governing equations were solved in a pressure-based transient solver. The gravity was considered (9.8 m/s^2). The PISO algorithm was employed for the pressure–velocity coupling, and the PRESTO and second-order upwind method were used to discretize the pressure and the momentum/energy equations, respectively. The predetermined convergence criteria for continuity, velocity and energy were 10^{-3}, 10^{-3}, and 10^{-6} respectively. The time step size was 0.2 s due to the previous CFD investigation.

3.2. Porous media model

The porous media model can be used for a wide variety of single phase and multiphase problems, including flow through packed beds, filter papers, perforated plates, flow distributors and tube banks. When using porous media model, the following assumptions are considered:

- The porosity of porous media is isotropic.
- In any conditions, only one pressure interpolation method is used in the porous media region.

Compared to the above mentioned momentum equation, a momentum source S_i is added in the porous media model, for simple homogenous porous media, the momentum source is as follow:

$$S_i = -\left(\frac{\mu}{\alpha} v_i + C_2 \frac{1}{2} \rho |v| v_i\right) \quad (1)$$

where, S_i is the momentum source in direction x, y, z. $|v|$ is the absolute value of velocity. C_2 is the inertial resistance, $1/\alpha$ is the viscous resistance.

In laminar flows through porous media, the porous media model reduces to Darcy's Law:

$$\nabla p = -\frac{\mu}{\alpha} \vec{v} \quad (2)$$

In this paper, the viscous resistance ($1/\alpha$) of the porous plate is calculated as 3.038×10^{10} m^{-2}, and the inertial resistance (C_2) is calculated as 1.575×10^{6} m^{-1}. The values have been indicated in Table 3.

3.3. Data analysis

The change of heat content (ΔHC) during a time step of Δt was determined by Eq. (3):

$$\Delta HC = (P_{in} - P_{out} - P_{heatloss}) \bullet \Delta t \tag{3}$$

P_{in}, P_{out} and $P_{heatloss}$ is the heat transfer rate [W] at inlet, outlet and tank surface respectively.

It was assumed that $HC = 0$ when the heat storage temperature is 30 °C.

The power (P) transferred to or from the heat storage was determined by Eq. (4):

$$P = P_{in} - P_{out} \tag{4}$$

The heat exchange capacity rate ($HXCR$) was determined by Eq. (5):

$$HXCR = -c_{p.water} \bullet \rho_{water} \bullet \dot{V} \bullet ln\left(1 - \frac{T_{in} - T_{out}}{T_{in} - T_{average}}\right) \tag{5}$$

4. Results and discussion

4.1. Model validation

The model was validated by comparing the outlet temperature measured and calculated. Fig. 6 shows the comparison between measured and calculated outlet temperatures and the charged heat in charging process. The calculated outlet temperature and charged heat have the same trend as the measured ones. The maximum difference between calculated outlet temperature and measured outlet temperature is less than 3 K. The maximum difference between calculated charged heat and measured charged heat is 0.4 kWh (1.8%). Based on the comparison, the accuracy of the CFD model was verified. The CFD model can be considered to be acceptable for the following analysis.

A detailed validation of the CFD model inclusive a grid independence investigation can be found in the previous publication of the authors [32].

4.2. Flow direction

4.2.1. Charge

The validated CFD model was used to investigate the influence of flow direction of the heat transfer fluid on its thermal performance. The temperature distributions of the heat storage during charge using either the top inlet (Top inlet mode, Case A-1) or the bottom inlet (Bottom inlet mode, Case A-2) are shown in Fig. 7. Apparently water temperatures in a horizontal plane of the heat storage in the Top Inlet Mode is more uniform than in the Bottom Inlet Mode. When using the Bottom Inlet Mode, due to the hot water short circuit flow, hot water gathered close to the outlet, resulting in smaller fluid velocity close to the inlet. Consequently there is an uneven temperature distribution on the horizontal plane of the storage. When using the Top Inlet Mode, the short circuit flow was totally eliminated. Hotter fluid tends to spread horizontally before being cooled down. The hot water heats the PCM tubes sufficiently before moving downwards. The reverse flow and the non-uniform heating of PCM tubes are also eliminated by using the Top Inlet Mode. A higher degree of thermal stratification is observed in the tank if the tank is charged via the top inlet.

The outlet temperatures and the charged heat of the heat storage with the Top Inlet and the Bottom Inlet are shown in the Fig. 8. The red curve indicates the Top Inlet mode, while the blue curve indicates the Bottom Inlet mode. During 0–39 min after the start of the charging, the outlet temperature in the Bottom Inlet mode is higher than that in the Top Inlet mode. That means, in the Bottom inlet mode, the inlet flow cannot release its heat completely, resulting in a lower charging efficiency. After 40 min, the outlet temperature in the Top Inlet mode was higher than that of Bottom Inlet mode. That means the storage tank with the top inlet had a higher charging efficiency or charging power than that with the bottom inlet. There is an interesting different point between the two modes. During 0–5 min, the outlet temperature in the Top Inlet mode was kept around 30 °C, however in the Bottom Inlet mode, the outlet temperature increased almost immediately when the charging process started. This means in the Top Inlet Mode, there was no short circuit flow. For the whole charging process, in the Top Inlet mode, it took the outlet temperature 60 min to reach 91.5 °C, while in the Bottom Inlet mode, it needed 100 min to reach 88.8 °C.

A comparison of the charged heat between the two modes is shown in Fig. 8. The storage tank with the top inlet had a faster increase of charged heat than that with the bottom inlet. For the whole charging process, when using the Top Inlet Mode, it took 55 min to store 23.5 kWh heat in the heat storage. In the Bottom Inlet Mode, it needed 100 min to charge 22.5 kWh heat in the heat storage. The Top Inlet Mode can store more heat while using less time. The difference is caused by the difference in temperature distributions. As shown in Fig. 7, the Top Inlet Mode has a higher degree of thermal stratification, consequently more heat was stored in the storage tank in the Top Inlet Mode. Comparing the two different HTF flow directions (two different inlet modes), the charging time of the Top Inlet mode is shorter than that of the Bottom Inlet mode, the charging process is shortened 50% by changing Bottom Inlet mode to Top Inlet mode. The charging time is defined as the time period of the outlet temperature changed from 30 °C to 88 °C.

The overlapping of fluid outlet temperatures in Fig. 8 is caused by the

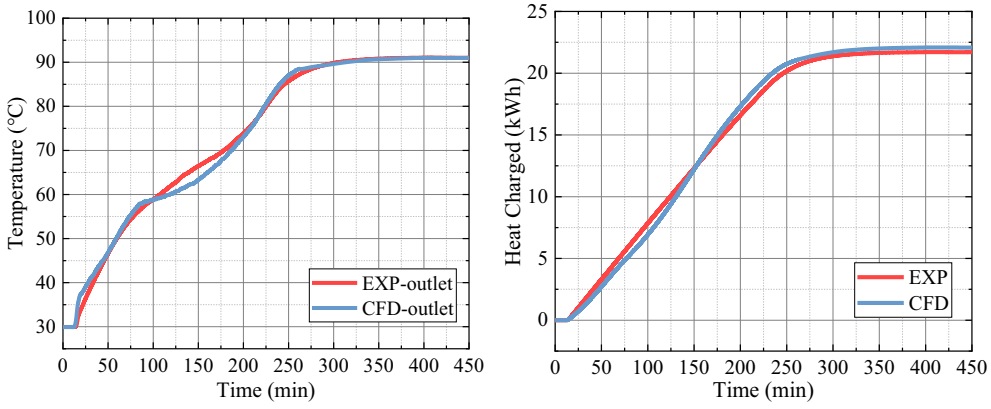

Fig. 6. Comparison between calculations and measurements during the charging process.

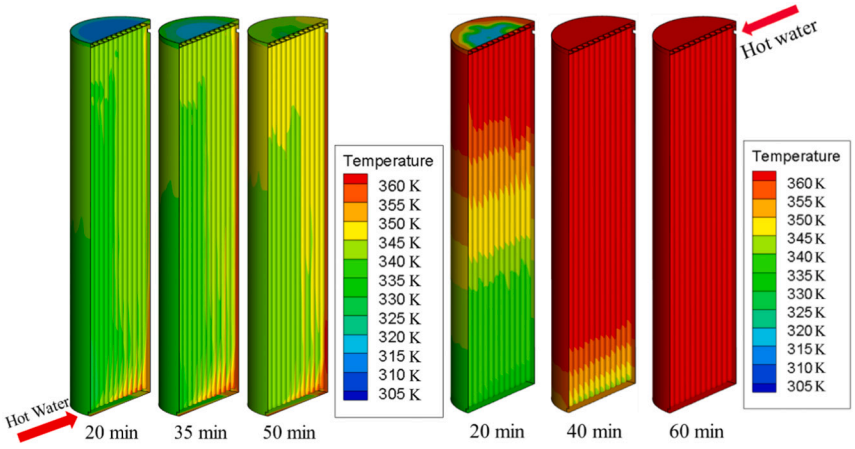

Fig. 7. Temperature distribution of the heat storage during charge: the Bottom inlet (Case A-2) (left) and the Top Inlet mode (Case A-1) (right).

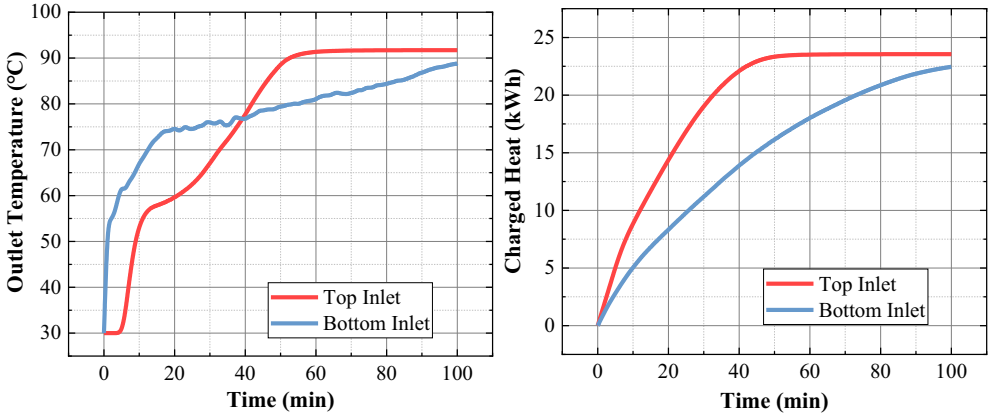

Fig. 8. Comparison of Top (Case A-1) and Bottom Inlet (Case A-2) Modes: outlet temperature and charged heat.

short circuit flow inside the heat storage during charge. In the start of the charging (0–40 min), due to the existence of the short circuit, the hot heat transfer fluid (HTF) in the storage with a bottom inlet leaves the heat storage before fully releasing heat, therefore, it has a higher outlet temperature and a lower heat exchange capacity rate than the storage with a top inlet (without short circuit flow). After 40 min, the PCM in the storage with a top inlet reaches a higher temperature, therefore, the outlet temperature of the HTF eventually exceeds that of the storage with a bottom inlet. The overlapping point is determined by the difference between the heat exchange capacity rates, which in turn is influenced by many factors, inclusive design of the storage, flow rate, flow pattern etc.

4.2.2. Discharge

Since the top inlet favors more the charge process than the discharge process, the CFD model was used to examine the influence of the flow direction on the discharge process. Fig. 9 and Fig. 10 show the temperature distribution of the heat storage during discharge of sensible heat process and discharge of latent heat process. In Fig. 10, the solidification was triggered at 10 min, and then the latent heat was released. When using the Top Inlet Mode in both discharges of sensible and latent heat, the cold water short circuit appeared seriously. When cold water enter the top inlet cold water could not distribute horizontally. Cold water vertically flowed down to the bottom of the heat storage, and then exited the heat storage through the bottom outlet.

Table 4 and Table 5 show thermal characteristic of the heat storage using the Top and the Bottom Inlet Mode in discharge of sensible and latent heat respectively. When using the Top Inlet Mode in the discharge

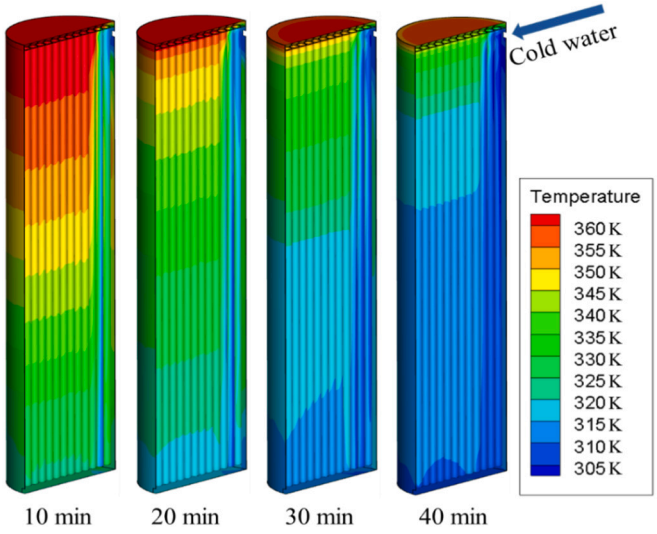

Fig. 9. Temperature distribution of the Top Inlet Mode during discharge of sensible heat (Case A-3).

process, the released heat will be reduced due to the cold water short circuit. Moreover, in the whole discharge process, the outlet temperature was low. The high-temperature heat was not able to be released.

In discharge of sensible heat, when changed from Top Inlet Mode to

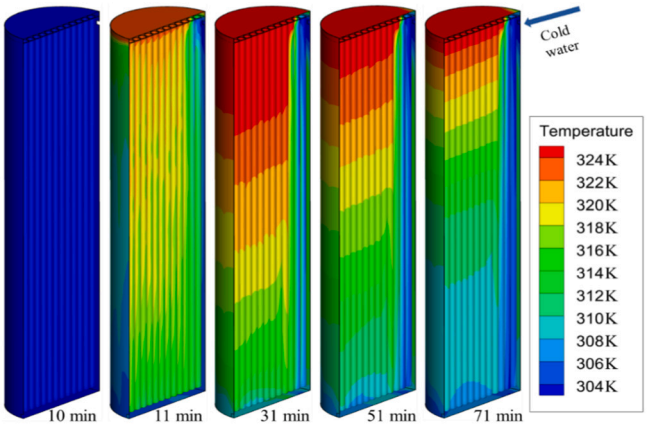

Fig. 10. Temperature distribution of the Top Inlet Mode during discharge of latent heat (Case A-5).

Table 4
Thermal characteristics of the heat storage during discharge of sensible heat.

Case	Modes	P^a (kW)	$HXCR^b$ (W/K)	Produced hot water (>40 °C)		
				Volume (L)	Average Temperature (°C)	Time (min)
A-3	Top Inlet	16.2	129	392	47.7	29
A-4	Bottom Inlet	41.6	807	294	68.2	21

[a] Energy weighted discharging power.
[b] Energy weighted HXCR.

Table 5
Thermal characteristics of the heat storage during discharge of latent heat process.

Case	Modes	P^a (kW)	$HXCR^b$ (W/K)	Produced hot water (>40 °C)		
				Volume (L)	Average Temperature (°C)	Time (min)
A-5	Top Inlet	4.3	457	0	–	–
A-6	Bottom Inlet	12.3	612	329	45.2	13

[a] Energy weighted discharging power.
[b] Energy weighted HXCR.

Bottom Inlet Mode, the discharge power was increased from 16.2 kW to 41.6 kW, the *HXCR* was increased from 129 W/K to 807 W/K. In discharge of latent heat, the power and *HXCR* of the Bottom Inlet mode was 12.3 kW and 612 W/K, obviously higher than 4.3 kW and 457 W/K which was achieved for the Top Inlet mode. In conclusion, the Top Inlet Mode should not be used in the discharge process.

From the comparison of the Top Inlet Mode and the Bottom Inlet Mode, the best operation mode can be recommended: In charge, the Top Inlet Mode should be used, while in discharge, the Bottom Inlet Mode should be used. In this condition, in the whole process of "charge-discharge of sensible heat-discharge of latent heat", the obvious thermal stratification can be formed inside the heat storage. The heat storage will have short charging time and large charged heat.

The needed time for one cycle of the Top Inlet Mode was more than 276 min, and that of the Bottom Inlet Mode was 271 min. The useful heat content of the heat storage for one cycle of the Top Inlet Mode was 23.5 kWh, and that of the Bottom Inlet Mode was 22.1 kWh. When using the Best Operation Mode, the useful heat content of the heat storage for one cycle was 23.5 kWh. The total time needed for one cycle was 196 min (55 min for charge, 45 min for discharge of sensible heat, 96 min for discharge of latent heat).

It should be pointed out that, to realize the optimized mode, additional equipment enabling change of flow direction is necessary. This will increase complexity and cost of the heat storage. Another important point is that, for the optimized mode, the heat storage may lose its stirring function. Inside the heat storage, the upper zone has higher temperature and the bottom part has lower temperature all the time, the convection inside the heat storage will be weak. The PCM is not able to be stirred by convection. This will increase the risk of phase separation.

In conclusion, if the PCM is stable enough, it is suggested to use the optimized mode: Top Inlet Mode in charge, Bottom Inlet Mode in discharge. If the PCM needs to be stirred during charge, it is suggested to use the Bottom Inlet Mode all the time.

4.3. Inlet size

The outlet temperatures and the average temperatures of the heat storage with different inlet sizes are shown in Fig. 11. The changes of outlet temperature and average temperature were similar in all inlet size conditions during charge. When charge started, the outlet temperature and average temperature increased immediately.

The difference of charging rates was small when the inlet size changing in each group. The results of 3.0 mm (Case B-7), 5.0 mm (Case B-8) and 8.0 (Case B-9) mm inlet sizes were close to each other. The results of 10.0 mm (Case B-10), 11.2 (Case B-11) mm and 12.0 (Case B-12) mm inlet sizes were close to each other. However, the change of charging rate was obvious when inlet size changing from the small inlets (3.0–8.0 mm) to the large inlets (10.0–12.0 mm). The difference between the results of 8.0 mm and 10.0 mm inlet sizes was large. This means there is a critical inlet size between 8.0 mm to 10.0 mm under the simulation condition.

The charged heat for the heat storage with different inlet sizes are shown in Fig. 12. During 0–100 min of the charging process, the charged heat with smaller inlet sizes (3.0, 5.0 and 8.0 mm) was larger than that of larger inlet sizes (10.0, 11.2 and 12.0 mm). When using the smaller inlet size, the heat storage stored 20 kWh energy in 51–55 min, while it took 67–75 min to store 20 kWh heat with a larger inlet size (10.0–12.0 mm). The charging rate of the heat storage increased with a decrease of the inlet size. Decreasing inlet size can increase the charging rate of the heat storage.

The temperature distributions of the heat storage with different inlet sizes are shown in Fig. 13. The symmetry plane of the heat storage is shown. From the figure, at 20 min, the results of 3.0 and 5.0 mm inlet sizes, there was almost no hot water short circuit, the temperature distributed uniformly.

For the 10.0 mm, 11.2 mm and 12.0 mm inlet sizes, the hot water short circuit appeared and increased with the increase of inlet size. When hot water entered the tank, the hot water was not mixed sufficiently before flowing upward because of buoyancy forces. The temperature inside the heat storage was not uniform, with high-temperature zone and middle-temperature zone separated. When using a large inlet size, since the heat storage did not have the "top-low and bottom-high" temperature distribution due to the serious short circuit flow of hot water, the heat storage may lose its stirring function.

The temperature distributions of the heat storage with different inlet sizes on the inlet and the outlet plane are shown in Fig. 14. With a decrease of the inlet size, the temperatures on the inlet and outlet plane became more uniform. The effect of decreasing inlet size was similar to the effect of increasing flow rate. The uniformity of temperature distribution could be improved, but not enough. Hot water was not fully mixed on the inlet plane before flowing upwards.

In conclusion, the small inlet size is suggested to make the uniform temperature distribution inside the heat storage. But the effect may not be sufficient. It should be pointed out that, in real applications, water pipes with standard dimensions should be used to connect the storage tank with the other components in the heating system. Fitting is need to connect the inlet/outlet to the connection pipes.

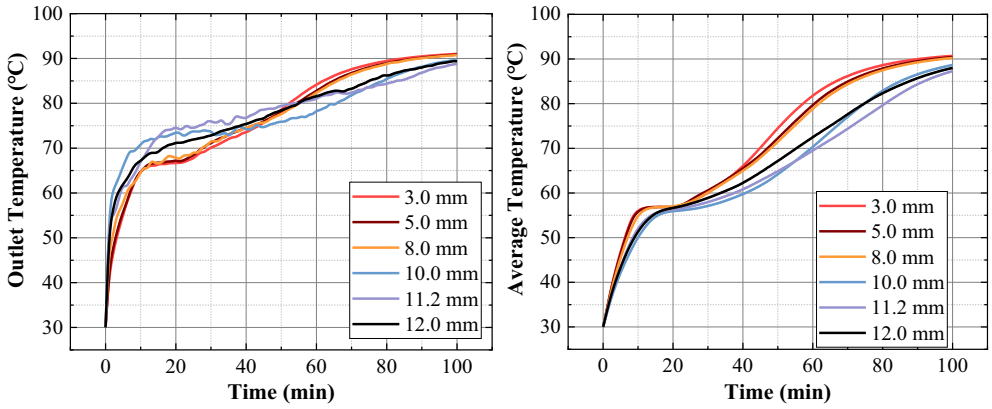

Fig. 11. The outlet temperatures and the average heat storage temperatures for different inlet sizes during charge.

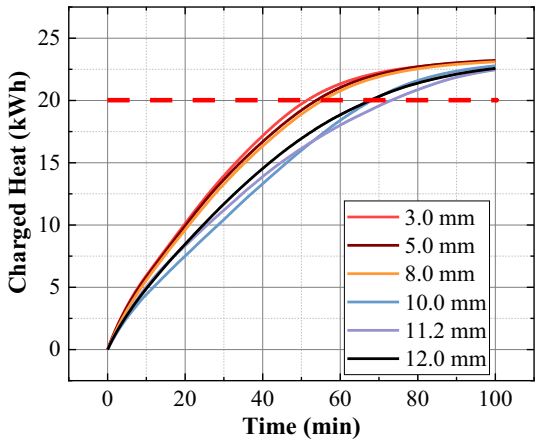

Fig. 12. The charged heat for the heat storage with different inlet sizes during charge.

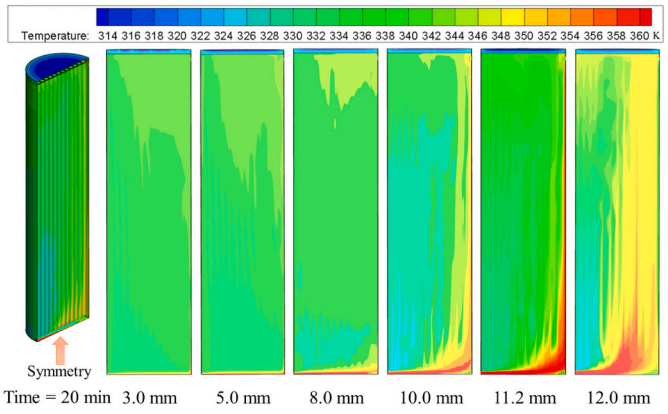

Fig. 13. The temperature distribution inside the heat storage with different inlet sizes during charge.

4.4. Porous plate

The outlet temperatures and the charged heat of the heat storage with and without a porous plate (Case C-13 and Case C-14) are shown in Fig. 15. Since hot water flowed out of the heat storage before fully releasing heat due to the short circuit flow, from the start to 52 min after the start of the charge, the outlet temperature of the heat storage without porous plate was higher than that of the heat storage with porous plate. The lower outlet temperature of the heat storage with the porous plate means that the short circuit flow inside the heat storage was reduced. After 52 min, the outlet temperature of the heat storage with the porous plate was higher. This means the temperature level of the heat storage with the porous plate was higher than that of the heat storage without porous plate. After 100 min, for the heat storage without the porous plate, the outlet temperature was 88.8 °C, while it is 91.7 °C for the heat storage with the porous plate.

For the charged heat of the heat storage with and without the porous plate, it is clear that after adding the porous plate, the charging rate was increased. For the heat storage without the porous plate, it needed 75 min to store 20 kWh heat, while it took 54 min for the heat storage with the porous plate to store 20 kWh heat. From the outlet temperature and the charged heat, the charging process of the heat storage was shortened by 28% by adding the porous plate.

As shown in Fig. 15, there is an overlapping point of the outlet temperatures with and without the porous plate, indicating an increase of heat exchange capacity rate by adding the porous plate. The porous plate ensures more even flow distribution after the incoming hot water enters into the bottom of the storage, increasing the heat exchange capacity of the storage. However, the trend of the overlapping point is difficult to predict as it is influenced by many factors.

The temperature distribution and path line distribution of water on the inlet plane are shown in Fig. 16. For the heat storage without the porous plate, on the inlet plane, hot water was not even distributed. The flow of hot water concentrated in the middle of the heat storage. After adding the porous plate, the hot water was even distributed after entering into the heat storage. The whole inlet plane had almost the same temperature.

The temperature distribution of the heat storage with the porous plate and the location of the porous plate are shown in Fig. 17. After adding the porous plate, the hot water short circuit was eliminated. The "bottom high-top low" temperature distribution was formed inside the heat storage. The hot water evenly distributed below the porous plate before entering the plate. The convection inside the PCM tubes was enhanced. The stirring function of the heat storage was achieved.

Adding the porous plate is an effective method to enhance the thermal performance of the heat storage. The pressure drop across the porous plate was marginal, meaning a lower flow resistance by the plate and an insignificant increase of pump power for flow circulation. The benefit is that, after adding a porous plate, the temperature distribution was improved and the temperature of the bottom part of the heat storage was increased. But it should be pointed out that, adding the porous plate will slightly increase the cost of the heat storage.

4.5. Comparison of the three storage designs

The results of the charging time and the charged heat of different

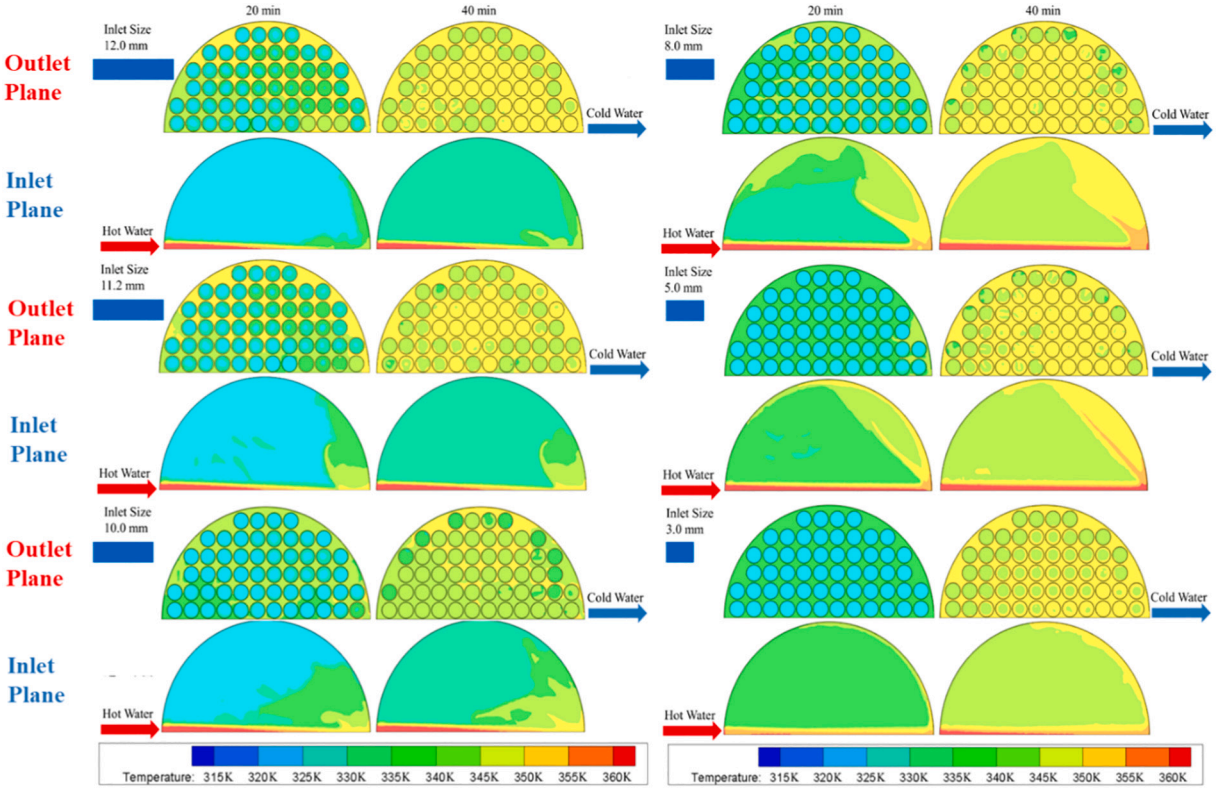

Fig. 14. The temperature distribution on the inlet plane and outlet plane under different inlet sizes in charge.

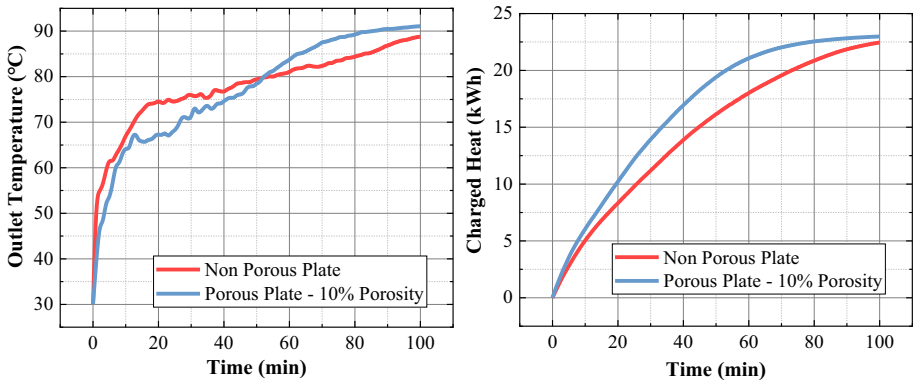

Fig. 15. Comparison of the outlet temperature and the charged heat between the two cases: With and without the porous plate.

designs are shown in Table 6. The results show that the heat storage with the Top Inlet Mode has the shortest charging time (32 min). The charging time of the heat storage with 3.0 mm, 5.0 mm and 8.0 mm inlet sizes and the heat storage with 10% porosity porous plate is 50–60 min. These designs can effectively increase the charging rate of the heat storage.

The charged heat of all simulations are in the range of 22.5–23.5 kWh. The difference is mainly caused by the different temperature distributions inside the heat storage. The heat storages with the Top Inlet Mode, 3.0 mm inlet size, 8.0 mm inlet size and 10% porosity porous plate have higher charged heat. Only the heat storage with the Top Inlet Mode and 10% porosity porous plate totally eliminated the short circuit flow inside the heat storage. Only the heat storage with 10% porosity porous plate can effectively achieve the stirring function for PCM.

The following suggestions are proposed for real applications of the investigated PCM-water heat storage:

- If the material cost is the concern of the heat storage, a larger water volume is recommended.
- If the tank volume is the concern of the heat storage, a larger PCM volume can obviously reduce the total volume of the storage.
- If the PCM is stable enough and the phase separation is not an issue, the optimized operation mode "Charge Top Inlet-Discharge Bottom Inlet" is recommended. There will be no short -circuit flow. The heat storage will have a short charging time and a high charged heat.
- If the PCM is not stable enough, the porous plate should be added in the heat storage. The stirring function can stir the PCM in liquid state, reducing phase separation of the PCM.
- If the inner structure of the heat storage cannot be changed, it is suggested to use small inlet size. The small inlet can reduce the short circuit flow and charging time, but the effect is limited.

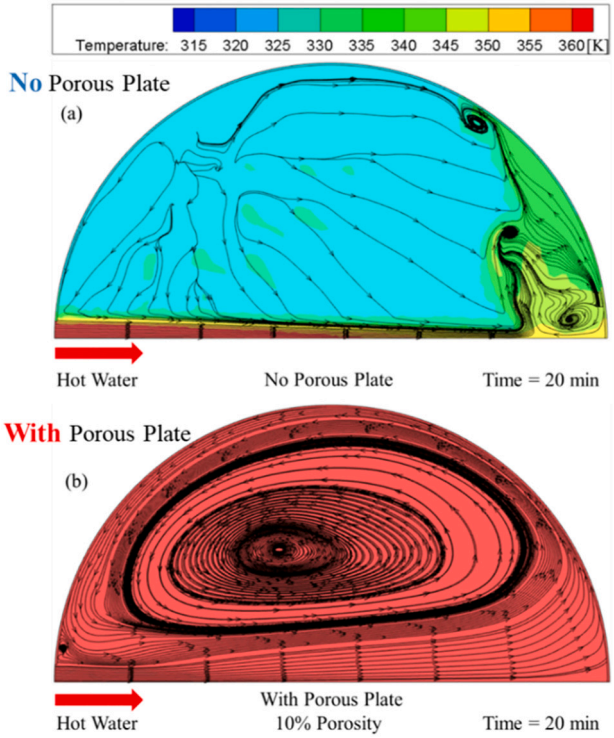

Fig. 16. Temperature distribution and path line distribution on Inlet Plane.

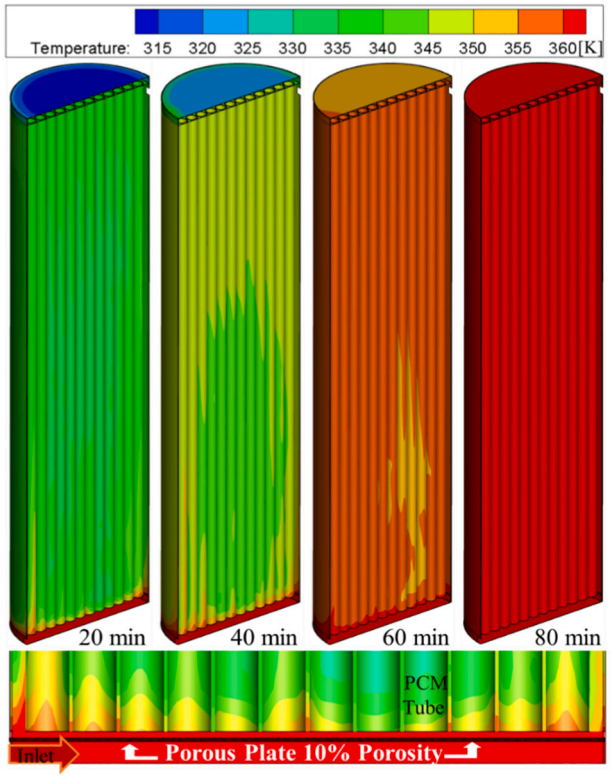

Fig. 17. Temperature distribution inside the heat storage with the porous plate.

5. Conclusion

A heat storage with 137.8 kg PCM and 75 L water was numerically investigated in this paper. The developed CFD model can accurately simulate the melting process, supercooling process and solidification process of the heat storage. The maximum difference between the calculated and the measured power transfers to and from the heat storage was less than 1.8%.

Calculations with the validated CFD model of the storage tank show that the short circuit flow existed inside the heat storage during charge. Due to the short circuit flow, the horizontal temperature distribution inside the heat storage was not uniform. The heat storage may lose its stirring function for the PCM in the tubes. Three different design improvements are investigated: Changing flow direction, changing inlet size and adding a porous plate inside the heat storage. The main findings are as follow:

Table 6
The charging characteristics of different design improvements.

Methods	Cases	Charging time [min][a]	Charged heat [kWh][b]	Short circuit
Change Flow Direction	Top Inlet	32	23.5	No
	Bottom Inlet	73	22.5	Yes
Change Inlet Size	3.0 mm	51	23.1	Yes
	5.0 mm	53	23.2	Yes
	8.0 mm	56	23.1	Yes
	10.0 mm	68	22.8	Yes
	11.2 mm	68	22.5	Yes
	12.0 mm	73	22.6	Yes
Add Porous Plate	Non Porous Plate	75	22.5	Yes
	10% Porosity Porous Plate	54	23.1	No

[a] The time of storing 20 kWh heat in charge.
[b] The charged heat at 100 min in charge.

- After moving the bottom inlet to the top of the storage, the charging time was shortened by 50%. The heat storage has short charging time (55 min) and large charged heat (23.5 kWh). However, the heat storage loses its stirring function for the PCM in the tubes.
- The charging time of the heat storage was reduced to 51 min by using 3.0 mm radius inlet, compared to 73 min by using 12.0 mm radius inlet. The small inlet size (3.0–8.0 mm) is suggested to achieve a uniform horizontal temperature distribution inside the heat storage. But the benefit is not large enough.
- The flow short circuit can be minimized by adding the 10% porosity porous plate. The stirring function is achieved by the "bottom high-top low" temperature distribution. The charging time of the heat storage is shortened by 28% from 75 min to 54 min. However extra material consumption and costs of the porous plate should be considered.

The findings of the paper will be used in further research. A TRNSYS model for the PCM heat storage will be developed based on the CFD results, which can be used to calculate performance of the PCM heat storage in a solar heating system.

Nomenclature

ρ	density [kg/m^3]
t	time [s]
$\vec{v}$	velocity [m/s]
μ	viscosity [Pa·s]
P	pressure [Pa]
$\vec{g}$	gravity [m/s^2]
β	liquid volume fraction
H	enthalpy [J, kWh]
L	latent heat [J/(g·K)]
T	temperature [K, °C]

Abbreviations

TES	thermal energy storage
PCM	phase change material
CFD	computational fluid dynamics
EXP	experiment
HTF	heat transfer fluid
SAT	sodium acetate trihydrate
HXCR	heat exchange capacity rate

CRediT authorship contribution statement

Gang Wang: Paper writing, research, editing.
Zhirong Liao: Reviewing.
Chao Xu: Reviewing.
Gerald Englmair: Reviewing.
Weiqiang Kong: Proofreading.
Jianhua Fan: Funding raising, proofreading, editing.
Gaosheng Wei: reviewing.
Simon Furbo: Reviewing, editing.

Declaration of competing interest

None.

Acknowledgments

The research was financed by the Danish Energy Agency EUDP project on participation of the IEA Task 58 'Material and Component Development for Thermal Energy Storage'. The research was partly funded by H.M. Heizkörper GmbH Heating Technology & Co. KG who developed the heat storage unit prototypes, partly supported by the National Natural Science Foundation of China (No. 52176069 and No. 51706071).

References

[1] J.M. Rueda-Cantuche, A.F. Amores, Consistent and unbiased carbon dioxide emission multipliers: performance of danish emission reductions via external trade, Ecol. Econ. 69 (2010) 988–998, https://doi.org/10.1016/j.ecolecon.2010.01.003.
[2] British Petroleum, Energy Outlook 2020 edition explores the forces shaping the global energy transition out to 2050 and the surrounding that, BP Energy Outlook 2030, Stat. Rev. London Br. Pet. (2020) 81. https://www.bp.com/content/dam/bp/business-sites/en/global/corporate/pdfs/energy-economics/energy-outlook/bp-energy-outlook-2020.pdf.
[3] P. Morseletto, F. Biermann, P. Pattberg, Governing by targets: reductio ad unum and evolution of the two-degree climate target, Int. Environ. Agreements Polit. Law Econ. 17 (2017) 655–676, https://doi.org/10.1007/s10784-016-9336-7.
[4] Z. Hausfather, R. Pearce, Analysis: WRI data suggests emissions have already 'peaked' in 49 countries, Carbon Br. (2020) 1–10.
[5] Y. Wang, C. Hui Guo, S. Rong Zhuang, X. Jie Chen, L. Qiong Jia, Z. Yu Chen, Z. Long Xia, Z. Wu, Major contribution to carbon neutrality by China's geosciences and geological technologies, China Geol. 4 (2021) 329–352, https://doi.org/10.31035/cg2021037.
[6] L. Li, X. Wang, Design and operation of hybrid renewable energy systems: current status and future perspectives, Curr. Opin. Chem. Eng. 31 (2021), 100669, https://doi.org/10.1016/j.coche.2021.100669.
[7] R. Elbahjaoui, Improvement of the thermal performance of a solar triple concentric-tube thermal energy storage unit using cascaded phase change materials, J. Energy Storage 42 (2021), 103047, https://doi.org/10.1016/j.est.2021.103047.
[8] Y. Heng, C. Lu, L. Yu, Z. Gao, The heterogeneous preferences for solar energy policies among US households, Energy Policy 137 (2020), 111187, https://doi.org/10.1016/j.enpol.2019.111187.
[9] L. Dong, T. Xing, J. Song, A. Yousefi, Performance analysis of a novel hybrid solar photovoltaic - pumped-hydro and compressed-air storage system in different climatic zones, J. Energy Storage 35 (2021), 102293, https://doi.org/10.1016/j.est.2021.102293.
[10] H. Ibrahim, A. Koca, Experimental Investigation of Water Flow Window System and Numerical Modeling of Solar Thermal Energy Storage With Phase Change Materials on the Way of Nearly Zero Energy Buildings 43, 2021, https://doi.org/10.1016/j.est.2021.103118.
[11] M. Caliano, N. Bianco, G. Graditi, L. Mongibello, Analysis of a phase change material-based unit and of an aluminum foam/phase change material composite-based unit for cold thermal energy storage by numerical simulation, Appl. Energy 256 (2019), 113921, https://doi.org/10.1016/j.apenergy.2019.113921.
[12] K.Y. Leong, S. Hasbi, B.A. Gurunathan, State of art review on the solidification and melting characteristics of phase change material in triplex-tube thermal energy storage, J. Energy Storage 41 (2021), 102932, https://doi.org/10.1016/j.est.2021.102932.
[13] J. Guo, J. Dong, B. Zou, H. Wang, L. Zhu, Y. Jiang, Experimental investigation on the effects of phase change material and different ventilation modes on the thermal storage, space heating and energy consumption characteristics of ventilated mortar blocks, J. Energy Storage 41 (2021), 102817, https://doi.org/10.1016/j.est.2021.102817.
[14] K.D. Poopalam, L. Raghunanan, L. Bouzidi, S.K. Yeong, S.S. Narine, Aliphatic fatty diamide as renewable phase change materials for thermal energy storage, J. Energy Storage 42 (2021), 102934, https://doi.org/10.1016/j.est.2021.102934.
[15] G. Wang, C. Xu, W. Kong, G. Englmair, J. Fan, G. Wei, S. Furbo, Review on sodium acetate trihydrate in flexible thermal energy storages: properties, challenges and applications, J. Energy Storage 40 (2021), 102780, https://doi.org/10.1016/j.est.2021.102780.
[16] H. Huang, J. Fan, J. Lin, Q. Zhao, Y. Zhang, Y. Xiao, Numerical phase change model considering crystal growth under supercooling, Appl. Therm. Eng. 200 (2021), 117685, https://doi.org/10.1016/j.applthermaleng.2021.117685.
[17] G. Wang, M. Dannemand, C. Xu, G. Englmair, S. Furbo, J. Fan, Thermal characteristics of a long-term heat storage unit with sodium acetate trihydrate, Appl. Therm. Eng. 187 (2021), 116563, https://doi.org/10.1016/j.applthermaleng.2021.116563.
[18] G. Zhou, M. Zhu, Y. Xiang, Effect of percussion vibration on solidification of supercooled salt hydrate PCM in thermal storage unit, Renew. Energy 126 (2018) 537–544, https://doi.org/10.1016/j.renene.2018.03.077.
[19] G. Zhou, Y. Xiang, Experimental investigations on stable supercooling performance of sodium acetate trihydrate PCM for thermal storage, Sol. Energy 155 (2017) 1261–1272, https://doi.org/10.1016/j.solener.2017.07.073.
[20] L. Yuan, Q. Ge, H. Fu, G. Jiang, Z. Yu, Q. Zheng, Y. Lv, J. Zhao, J. Yu, Sodium acetate trihydrate-crystallization inhibitor system for seasonal latent heat storage, J. Energy Eng. 144 (2018) 4018022.
[21] J.B. Johansen, M. Dannemand, W. Kong, J. Fan, J. Dragsted, S. Furbo, Thermal conductivity enhancement of sodium acetate trihydrate by adding graphite powder and the effect on stability of supercooling, Energy Procedia 70 (2015) 249–256, https://doi.org/10.1016/j.egypro.2015.02.121.
[22] M. Dannemand, J. Dragsted, J. Fan, J.B. Johansen, W. Kong, S. Furbo, Experimental investigations on prototype heat storage units utilizing stable supercooling of sodium acetate trihydrate mixtures, Appl. Energy 169 (2016) 72–80, https://doi.org/10.1016/j.apenergy.2016.02.038.
[23] G. Englmair, C. Moser, S. Furbo, M. Dannemand, J. Fan, Design and functionality of a segmented heat-storage prototype utilizing stable supercooling of sodium acetate trihydrate in a solar heating system, Appl. Energy 221 (2018) 522–534, https://doi.org/10.1016/j.apenergy.2018.03.124.
[24] G. Englmair, W. Kong, J. Brinkø Berg, S. Furbo, J. Fan, Demonstration of a solar combi-system utilizing stable supercooling of sodium acetate trihydrate for heat storage, Appl. Therm. Eng. 166 (2020), 114647, https://doi.org/10.1016/j.applthermaleng.2019.114647.
[25] Z. Elmaazouzi, I.A. Laasri, A. Gounni, M. El Alami, E.G. Bennouna, Enhanced thermal performance of finned latent heat thermal energy storage system: fin parameters optimization, J. Energy Storage 43 (2021), 103116, https://doi.org/10.1016/j.est.2021.103116.
[26] M. Kirincic, A. Trp, K. Lenic, Numerical evaluation of the latent heat thermal energy storage performance enhancement by installing longitudinal fins, J. Energy Storage 42 (2021), 103085, https://doi.org/10.1016/j.est.2021.103085.
[27] J. Wu, Q. Chen, Y. Zhang, K. Sun, A novel compensating fins configuration for improving the thermal performance of latent heat thermal energy storage unit, J. Energy Storage 44 (2021), 103328, https://doi.org/10.1016/j.est.2021.103328.
[28] C. Yu, S. Wu, Y. Huang, F. Yao, X. Liu, Charging performance optimization of a latent heat storage unit with fractal tree-like fins, J. Energy Storage 30 (2020), 101498, https://doi.org/10.1016/j.est.2020.101498.
[29] B. Lamrani, T. Kousksou, Numerical investigation of a shell-and-tube latent heat thermal energy storage system for urban heating network, J. Energy Storage 43 (2021), 103216, https://doi.org/10.1016/j.est.2021.103216.
[30] V. Joshi, C. Wasnik, A. Wadegaonkar, S.B. Kedare, M. Bose, Influence of porosity and permeability of flow distributor on thermal stratification in single media storage tank, J. Energy Storage 44 (2021), 103241, https://doi.org/10.1016/j.est.2021.103241.
[31] J. Weiss, I. Ortega-Fernández, R. Müller, D. Bielsa, T. Fluri, Improved thermocline initialization through optimized inlet design for single-tank thermal energy storage systems, J. Energy Storage. 42 (2021), 103088, https://doi.org/10.1016/j.est.2021.103088.
[32] G. Wang, C. Xu, G. Englmair, W. Kong, J. Fan, S. Furbo, G. Wei, Experimental and numerical study of a latent heat storage using sodium acetate trihydrate for short and long term applications, J. Energy Storage (2021), 103588, https://doi.org/10.1016/j.est.2021.103588.
[33] W. Youssef, Y.T. Ge, S.A. Tassou, CFD modelling development and experimental validation of a phase change material (PCM) heat exchanger with spiral-wired tubes, Energy Convers. Manag. 157 (2018) 498–510, https://doi.org/10.1016/j.enconman.2017.12.036.